Improved test of the flavor independence of strong interactions

K. Abe,[2] K. Abe,[19] T. Abe,[27] I. Adam,[27] T. Akagi,[27] N. J. Allen,[4] A. Arodzero,[20] W. W. Ash,[27] D. Aston,[27] K. G. Baird,[15] C. Baltay,[37] H. R. Band,[36] M. B. Barakat,[14] O. Bardon,[17] T. L. Barklow,[27] J. M. Bauer,[16] G. Bellodi,[21] R. Ben-David,[37] A. C. Benvenuti,[3] G. M. Bilei,[23] D. Bisello,[22] G. Blaylock,[15] J. R. Bogart,[27] B. Bolen,[16] G. R. Bower,[27] J. E. Brau,[20] M. Breidenbach,[27] W. M. Bugg,[30] D. Burke,[27] T. H. Burnett,[35] P. N. Burrows,[21] A. Calcaterra,[11] D. O. Caldwell,[32] D. Calloway,[27] B. Camanzi,[10] M. Carpinelli,[24] R. Cassell,[27] R. Castaldi,[24] A. Castro,[22] M. Cavalli-Sforza,[33] A. Chou,[27] E. Church,[35] H. O. Cohn,[30] J. A. Coller,[5] M. R. Convery,[27] V. Cook,[35] R. Cotton,[4] R. F. Cowan,[17] D. G. Coyne,[33] G. Crawford,[27] C. J. S. Damerell,[25] M. N. Danielson,[7] M. Daoudi,[27] N. de Groot,[27] R. Dell'Orso,[23] P. J. Dervan,[4] R. de Sangro,[11] M. Dima,[9] A. D'Oliveira,[6] D. N. Dong,[17] P. Y. C. Du,[30] R. Dubois,[27] B. I. Eisenstein,[12] V. Eschenburg,[16] E. Etzion,[36] S. Fahey,[7] D. Falciai,[11] C. Fan,[7] J. P. Fernandez,[33] M. J. Fero,[17] K. Flood,[15] R. Frey,[20] T. Gillman,[25] G. Gladding,[12] S. Gonzalez,[17] E. L. Hart,[30] J. L. Harton,[9] A. Hasan,[4] K. Hasuko,[31] S. J. Hedges,[5] S. S. Hertzbach,[15] M. D. Hildreth,[27] J. Huber,[20] M. E. Huffer,[27] E. W. Hughes,[27] X. Huynh,[27] H. Hwang,[20] M. Iwasaki,[20] D. J. Jackson,[25] P. Jacques,[26] J. A. Jaros,[27] Z. Y. Jiang,[27] A. S. Johnson,[27] J. R. Johnson,[36] R. A. Johnson,[6] T. Junk,[27] R. Kajikawa,[19] M. Kalelkar,[26] Y. Kamyshkov,[30] H. J. Kang,[26] L. Karliner,[12] H. Kawahara,[27] Y. D. Kim,[28] R. King,[27] M. E. King,[27] R. R. Kofler,[15] N. M. Krishna,[7] R. S. Kroeger,[16] M. Langston,[20] A. Lath,[17] D. W. G. Leith,[27] V. Lia,[17] C.-J. S. Lin,[27] X. Liu,[33] M. X. Liu,[37] M. Loreti,[22] A. Lu,[32] H. L. Lynch,[27] J. Ma,[35] G. Mancinelli,[26] S. Manly,[37] G. Mantovani,[23] T. W. Markiewicz,[27] T. Maruyama,[27] H. Masuda,[27] E. Mazzucato,[10] A. K. McKemey,[4] B. T. Meadows,[6] G. Menegatti,[10] R. Messner,[27] P. M. Mockett,[35] K. C. Moffeit,[27] T. B. Moore,[37] M. Morii,[27] D. Muller,[27] V. Murzin,[18] T. Nagamine,[31] S. Narita,[31] U. Nauenberg,[7] H. Neal,[27] M. Nussbaum,[6] N. Oishi,[19] D. Onoprienko,[30] L. S. Osborne,[17] R. S. Panvini,[34] H. Park,[20] C. H. Park,[29] T. J. Pavel,[27] I. Peruzzi,[11] M. Piccolo,[11] L. Piemontese,[10] E. Pieroni,[24] K. T. Pitts,[20] R. J. Plano,[26] R. Prepost,[36] C. Y. Prescott,[27] G. D. Punkar,[27] J. Quigley,[17] B. N. Ratcliff,[27] T. W. Reeves,[34] J. Reidy,[16] P. L. Reinertsen,[33] P. E. Rensing,[27] L. S. Rochester,[27] P. C. Rowson,[8] J. J. Russell,[27] O. H. Saxton,[27] T. Schalk,[33] R. H. Schindler,[27] B. A. Schumm,[33] J. Schwiening,[27] S. Sen,[37] V. V. Serbo,[36] M. H. Shaevitz,[8] J. T. Shank,[5] G. Shapiro,[13] D. J. Sherden,[27] K. D. Shmakov,[30] C. Simopoulos,[27] N. B. Sinev,[20] S. R. Smith,[27] M. B. Smy,[9] J. A. Snyder,[37] H. Staengle,[9] A. Stahl,[27] P. Stamer,[26] R. Steiner,[1] H. Steiner,[13] M. G. Strauss,[15] D. Su,[27] F. Suekane,[31] A. Sugiyama,[19] S. Suzuki,[19] M. Swartz,[27] A. Szumilo,[35] T. Takahashi,[27] F. E. Taylor,[17] J. Thom,[27] E. Torrence,[17] N. K. Toumbas,[27] A. I. Trandafir,[15] J. D. Turk,[37] T. Usher,[27] C. Vannini,[24] J. Va'vra,[27] E. Vella,[27] J. P. Venuti,[34] R. Verdier,[17] P. G. Verdini,[24] S. R. Wagner,[27] D. L. Wagner,[7] A. P. Waite,[27] S. Walston,[20] J. Wang,[27] C. Ward,[4] S. J. Watts,[4] A. W. Weidemann,[30] E. R. Weiss,[35] J. S. Whitaker,[5] S. L. White,[30] F. J. Wickens,[25] B. Williams,[7] D. C. Williams,[17] S. H. Williams,[27] S. Willocq,[27] R. J. Wilson,[9] W. J. Wisniewski,[27] J. L. Wittlin,[15] M. Woods,[27] G. B. Word,[34] T. R. Wright,[36] J. Wyss,[22] R. K. Yamamoto,[17] J. M. Yamartino,[17] X. Yang,[20] J. Yashima,[31] S. J. Yellin,[32] C. C. Young,[27] H. Yuta,[2] G. Zapalac,[36] R. W. Zdarko,[27] and J. Zhou[20]

(The SLD Collaboration)

[1]*Adelphi University, South Avenue, Garden City, New York 11530*

[2]*Aomori University, 2-3-1 Kohata, Aomori City, 030 Japan*

[3]*INFN Sezione di Bologna, Via Irnerio 46, I-40126 Bologna, Italy*

[4]*Brunel University, Uxbridge, Middlesex, UB8 3PH United Kingdom*

[5]*Boston University, 590 Commonwealth Avenue, Boston, Massachusetts 02215*

[6]*University of Cincinnati, Cincinnati, Ohio 45221*

[7]*University of Colorado, Campus Box 390 Boulder, Colorado 80309*

[8]*Columbia University, Nevis Laboratories P.O. Box 137 Irvington, New York 10533*

[9]*Colorado State University, Fort Collins, Colorado 80523*

[10]*INFN Sezione di Ferrara, Via Paradiso 12, I-44100 Ferrara, Italy*

[11]*Laboratori Nazionali di Frascati, Casella Postale 13, I-00044 Frascati, Italy*

[12]*University of Illinois, 1110 West Green Street, Urbana, Illinois 61801*

[13]*Lawrence Berkeley Laboratory, Department of Physics 50B-5211, University of California, Berkeley, California 94720*

[14]*Louisiana Technical University, Ruston, Louisiana 71272*

[15]*University of Massachusetts, Amherst, Massachusetts 01003*

[16]*University of Mississippi, University, Mississippi 38677*

[17]*Massachusetts Institute of Technology, 77 Massachusetts Avenue, Cambridge, Massachusetts 02139*

[18]*Moscow State University, Institute of Nuclear Physics, 119899 Moscow, Russia*

[19]*Nagoya University, Nagoya 464, Japan*

[20]*University of Oregon, Department of Physics, Eugene, Oregon 97403*

[21]*Oxford University, Oxford, OX1 3RH, United Kingdom*

[22]*Universita di Padova, Via F. Marzolo, 8 I-35100 Padova, Italy*

[23]*Universita di Perugia, Sezione INFN, Via A. Pascoli, I-06100 Perugia, Italy*
[24]*INFN, Sezione di Pisa, Via Livornese, 582/AS Piero a Grado I-56010, Pisa, Italy*
[25]*Rutherford Appleton Laboratory, Chiton, Didcot, Oxon OX11 0QX, United Kingdom*
[26]*Rutgers University, Serin Physics Laboratories, Piscataway, New Jersey 08855-0849*
[27]*Stanford Linear Accelerator Center, 2575 Sand Hill Road, Menlo Park, California 94025*
[28]*Sogang University, Ricci Hall, Seoul, Korea*
[29]*Soongsil University, Dongjakgu Sangdo 5 dong 1-1, Seoul, Korea 156-743*
[30]*University of Tennessee, 401 A.H. Nielsen Physics Building, Knoxville, Tennessee 37996-1200*
[31]*Tohoku University, Bubble Chamber Laboratory Aramaki, Sendai 980 Japan*
[32]*University of California at Santa Barbara, 3019 Broida Hall, Santa Barbara, California 93106*
[33]*University of California at Santa Cruz, Santa Cruz, California 95064*
[34]*Vanderbilt University, Stevenson Center, Room 5333, P.O. Box 1807, Station B, Nashville, Tennessee 37235*
[35]*University of Washington, Seattle, Washington 98105*
[36]*University of Wisconsin, 1150 University Avenue, Madison, Wisconsin 53706*
[37]*Yale University, 5th Floor Gibbs Laboratory, P.O. Box 208121, New Haven, Connecticut 06520-8121*

(Received 7 April 1998; published 17 November 1998)

We present an improved comparison of the strong coupling of the gluon to light ($q_l = u+d+s$), c, and b quarks, determined from multijet rates in flavor-tagged samples of hadronic Z^0 decays recorded with the SLC Large Detector at the SLAC Linear Collider between 1993 and 1995. Flavor separation among primary $q_l\overline{q_l}$, $c\overline{c}$, and $b\overline{b}$ final states was made on the basis of the reconstructed mass of long-lived heavy-hadron decay vertices, yielding tags with high purity and low bias against $\geqslant$ 3-jet final states. We find: $\alpha_s^c/\alpha_s^{uds} = 1.036 \pm 0.043(\text{stat})^{+0.041}_{-0.045}(\text{syst})^{+0.020}_{-0.018}(\text{theory})$ and $\alpha_s^b/\alpha_s^{uds} = 1.004 \pm 0.018(\text{stat})^{+0.026}_{-0.031}(\text{syst})^{+0.018}_{-0.029}(\text{theory})$. [S0556-2821(98)01621-X]

PACS number(s): 12.38.Qk, 13.38.Dg

I. INTRODUCTION

In order for quantum chromodynamics (QCD) [1] to be a gauge-invariant renormalizable field theory, it is required that the strong coupling between quarks (q) and gluons (g), α_s, be independent of quark flavor. This basic ansatz can be tested directly in e^+e^- annihilation by measuring the strong coupling in events of the type $e^+e^- \to q\overline{q}g$ for specific quark flavors. Whereas an absolute determination of α_s using such a technique is limited, primarily by large theoretical uncertainties, to the 5% level of precision [2], a much more precise test of the flavor independence can be made from the ratio of the couplings for different quark flavors, in which most experimental errors and theoretical uncertainties cancel. Furthermore, the emission of gluon radiation in $b\overline{b}$ events is expected [3] to be modified relative to that in $q_l\overline{q_l}$ ($q_l = u+d+s$) events due to the large b-quark mass, and comparison of the rates for $Z^0 \to b\overline{b}g$ and $Z^0 \to q_l\overline{q_l}g$ may allow measurement of the running mass[1] of the b quark,[2] $m_b(M_{Z^0})$. Finally, in addition to providing a powerful test of QCD, such measurements allow constraints to be placed on physics beyond the standard model. For example, a flavor-dependent anomalous quark chromomagnetic moment would modify [6] the emission rate of gluons for the different quark flavors, and would manifest itself in the form of an apparently flavor-dependent strong coupling.

The first such comparisons, of α_s for c or b quarks with α_s for all flavors, were made at the DESY e^+e^- collider PETRA at c.m. energies in the range $35 \leqslant \sqrt{s} \leqslant 47$ GeV and were limited in precision to $\delta\alpha_s^c/\alpha_s^{all} = 0.41$ and $\delta\alpha_s^b/\alpha_s^{all} = 0.57$ [7] due to the small data sample and limited heavy-quark tagging capability. These studies made the simplifying assumptions that $\alpha_s^b = \alpha_s^{uds}$ and $\alpha_s^c = \alpha_s^{uds}$, respectively. More recently, measurements made at the Z^0 resonance have benefitted from the use of micro vertex detectors for improved heavy-quark tagging. Samples of tagged $b\overline{b}$ events recorded at the CERN e^+e^- collider LEP have been used to test flavor-independence to a precision of $\delta\alpha_s^b/\alpha_s^{all} = 0.012$ [8,9], but these measurements were insensitive to any differences among α_s values for the non-b-quarks. The ALEPH Collaboration also measured $\alpha_s^{bc}/\alpha_s^{uds}$ to a precision of ± 0.023 [9], but in this case there is no sensitivity to a different α_s for c and b quarks.

The OPAL Collaboration has measured $\alpha_s^f/\alpha_s^{all}$ for all five flavors f with no assumption on the relative value of α_s for the different flavors [10], and has verified flavor-independence to a precision of $\delta\alpha_s^b/\alpha_s^{all} = 0.026$, $\delta\alpha_s^c/\alpha_s^{all} = 0.09$, $\delta\alpha_s^s/\alpha_s^{all} = 0.15$, $\delta\alpha_s^d/\alpha_s^{all} = 0.20$, and $\delta\alpha_s^u/\alpha_s^{all} = 0.21$. In that analysis the precision of the test was limited by the kinematic signatures used to tag c and light-quark events, which suffer from low efficiency and strong biases against events containing hard gluon radiation. In our previous study [11], we used hadron lifetime information as a basis for separation of $b\overline{b}$, $c\overline{c}$ and light-quark events with

[1]Use of the modified minimal subtraction renormalization scheme [4] is implied throughout this paper.

[2]The DELPHI Collaboration has recently measured the three-jet rate ratio R_3^b/R_3^{uds} to a precision of ± 0.009, and, under the assumption of a flavor-independent strong coupling, derived a value of the running b-mass [5]; this issue will be discussed in Sec. VI.

relatively small bias against 3-jet final states. We verified flavor-independence to a precision of $\delta\alpha_s^b/\alpha_s^{all}=0.06$, $\delta\alpha_s^c/\alpha_s^{all}=0.17$, and $\delta\alpha_s^{uds}/\alpha_s^{all}=0.04$.

Here we present an improved test of the flavor-independence of strong interactions using a sample of hadronic Z^0 decay events produced by the SLAC Linear Collider (SLC) and recorded in the SLC Large Detector (SLD) in data-taking runs between 1993 and 1995. The precise tracking capability of the Central Drift Chamber and the 120-million-pixel CCD-based Vertex Detector (VXD2), combined with the stable, micron-sized beam interaction point (IP), allowed us to reconstruct topologically secondary vertices from heavy-hadron decays with high efficiency. High-purity samples of $Z^0\to b\bar{b}(g)$ and $Z^0\to c\bar{c}(g)$ events were then tagged on the basis of the reconstructed mass and momentum of the secondary vertex. Events containing no secondary vertex and no tracks significantly displaced from the IP were tagged as a high-purity $Z^0\to q_l\bar{q}_l(g)$ event sample. The method makes no assumptions about the relative values of α_s^b, α_s^c and α_s^{uds}. Furthermore, an important advantage of the method is that it has low bias against $\geqslant$3-jet events. In addition to using an improved flavor-tagging technique, this analysis utilizes a data sample three times larger than that used for our previous measurement, and allows us to test the flavor independence of strong interactions to a precision higher by roughly a factor of three. Finally, quark mass effects in $Z^0\to q\bar{q}g$ events have recently been calculated [12,13] at next-to-leading order in perturbative QCD, and are non-negligible on the scale of our experimental errors; we have utilized these calculations in this analysis.

II. APPARATUS AND HADRONIC EVENT SELECTION

This analysis is based on roughly 150,000 hadronic events produced in e^+e^- annihilations at a mean center-of-mass energy of $\sqrt{s}=91.28$ GeV. A general description of the SLD can be found elsewhere [14]. The trigger and initial selection criteria for hadronic Z^0 decays are described in Ref. [15]. This analysis used charged tracks measured in the Central Drift Chamber (CDC) [16] and in the Vertex Detector (VXD2) [17]. Momentum measurement is provided by a uniform axial magnetic field of 0.6T. The CDC and VXD2 give a momentum resolution of $\sigma_{p_\perp}/p_\perp=0.01\oplus 0.0026p_\perp$, where $p_\perp$ is the track momentum transverse to the beam axis in GeV/c. In the plane normal to the beamline, the centroid of the micron-sized SLC IP was reconstructed from tracks in sets of approximately thirty sequential hadronic Z^0 decays to a precision of $\sigma_{IP}\simeq 7\ \mu$m. Including the uncertainty on the IP position, the resolution on the charged-track impact parameter (d) projected in the plane perpendicular to the beamline is $\sigma_d=11\oplus 70/(p_\perp\sin^{3/2}\theta)\ \mu$m, where θ is the track polar angle with respect to the beamline. The event thrust axis [18] was calculated using energy clusters measured in the Liquid Argon Calorimeter [19].

A set of cuts was applied to the data to select well-measured tracks and events well contained within the detector acceptance. Charged tracks were required to have a distance of closest approach transverse to the beam axis within 5 cm, and within 10 cm along the axis from the measured IP, as well as $|\cos\theta|<0.80$, and $p_\perp>0.15$ GeV/c. Events were required to have a minimum of seven such tracks, a thrust axis polar angle with respect to the beamline, θ_T, within $|\cos\theta_T|<0.71$, and a charged visible energy $E_{\rm vis}$ of at least 20 GeV, which was calculated from the selected tracks assigned the charged pion mass. The efficiency for selecting a well-contained $Z^0\to q\bar{q}(g)$ event was estimated to be above 96% independent of quark flavor. The selected sample comprised 77 896 events, with an estimated $0.10\pm 0.05\%$ background contribution dominated by $Z^0\to\tau^+\tau^-$ events.

For the purpose of estimating the efficiency and purity of the event flavor-tagging procedure, we made use of a detailed Monte Carlo (MC) simulation of the detector. The JETSET 7.4 [20] event generator was used, with parameter values tuned to hadronic e^+e^- annihilation data [21], combined with a simulation of B-hadron decays tuned [22] to $\Upsilon(4S)$ data and a simulation of the SLD based on GEANT 3.21 [23]. Inclusive distributions of single-particle and event-topology observables in hadronic events were found to be well described by the simulation [15]. Uncertainties in the simulation were taken into account in the systematic errors (Sec. V).

III. FLAVOR TAGGING

Separation of the accepted event sample into tagged flavor subsamples was based on the invariant mass of topologically reconstructed long-lived heavy-hadron decay vertices, as well as on charged-track impact parameters in the plane normal to the beamline. In each event a jet structure was defined as a basis for flavor-tagging by applying the JADE jet-finding algorithm [24] to the selected tracks; a value of the normalized jet-jet invariant-mass parameter $y_c=0.02$ was used. The impact parameter of each track, d, was given a positive (negative) sign according to whether the point-of-closest approach to its jet axis was on the same side (opposite side) of the IP as the jet. Charged tracks used for the subsequent event flavor-tagging were further required to have at least 40 hits in the CDC, with the first hit at a radial distance of less than 39 cm from the beamline, at least one VXD2 hit, a combined CDC+VXD2 track fit quality of $\chi^2_{dof}<5$, momentum $p>0.5$ GeV/c, a distance of closest approach transverse to the beam axis within 0.3 cm, and within 1.5 cm along the axis from the measured IP, and an error on the impact parameter, σ_d, less than 250 μm. Tracks from identified K^0_s and Λ decays and γ conversions were removed.

In each jet we then searched for a secondary vertex (SV), namely a vertex spatially separated from the measured IP. In the search those tracks were considered that were assigned to the jet by the jet-finder. Individual track probability-density functions in three-dimensional co-ordinate space were examined and a candidate SV was defined by a region of high track overlap density; the method is described in detail in [25]. A SV was required to contain two or more tracks, and to be separated from the IP by at least 1 mm. We found 14 096 events containing a SV in only one jet, 5817 events containing a SV in two jets, and 54 events containing a SV in more than two jets. The selected SVs comprise, on average,

3.0 tracks. These requirements preferentially select SVs that originate from the decay of particles with relatively long lifetime. In our simulated event sample, a SV was found in 50% of all true b-quark hemispheres, in 15% of true c-quark, and in $<1\%$ of true light-quark hemispheres [25], where hemispheres were defined by the plane normal to the thrust axis that contains the IP.

Due to the cascade structure of B-hadron decays, not all the tracks in the decay chain will necessarily originate from a common decay point, and in such cases the SV may not be fully reconstructed in $b\bar{b}$ events. Therefore, we improved our estimate of the SV by allowing the possibility of attaching additional tracks. First, we defined the vertex axis to be the straight line joining the IP and the SV centroids, and D to be the distance along this axis between the IP and the SV. For each track in the jet not included in the SV, the point of closest approach (POCA), and corresponding distance of closest approach, T, to the vertex axis were determined. The length, L, of the projection of the vector joining the IP and the POCA, along the vertex axis was then calculated. Tracks with $T<1.0$ mm, $L>0.8$ mm and $L/D>0.22$ were then attached to the SV. On average 0.5 tracks per SV were attached in this fashion.

The invariant mass, M_{ch}, of each SV was then calculated by assigning each track the charged pion mass. In order to account partially for the effect of neutral particles missing from the SV, we applied a kinematic correction to the calculated M_{ch}. We added the momentum vectors of all tracks forming the SV to obtain the vertex momentum, $P_{vtx}^{\rightarrow}$, and evaluated the magnitude of the component of the vertex momentum tranverse to the vertex axis, P_t. In order to reduce the effect of the IP and SV measurement errors, the vertex axis was varied within an envelope defined by all possible cotangents to the error ellipsoids of both the IP and the SV, and the minimum P_t was chosen. We then defined the P_t-corrected vertex mass, $M_{vtx}=\sqrt{M_{ch}^2+P_t^2}+|P_t|$.

The distributions of M_{vtx} and P_{vtx} are shown in Fig. 1; the data are reproduced by the simulation, in which the primary event-flavor breakdown is indicated. The region $M_{vtx}>2$ GeV/c^2 is populated predominantly by $Z^0\rightarrow b\bar{b}$ events, whereas the region $M_{vtx}\leq 2$ GeV/c^2 is populated roughly equally by $b\bar{b}$ and non-$b\bar{b}$ events.

In order to optimize the separation among flavors, we examined the two-dimensional distribution of P_{vtx} vs M_{vtx}. The distribution for events containing a SV is shown in Fig. 2 for the data and simulated samples; the data (Fig. 2a) are reproduced by the simulation (Fig. 2b). The distributions for the simulated subsamples corresponding to true primary $b\bar{b}$, $c\bar{c}$, and $q_l\bar{q}_l$ events are shown in Figs. 2c, 2d and 2e, respectively.

In order to separate $b\bar{b}$ and $c\bar{c}$ events from each other, and from the $q_l\bar{q}_l$ events, we defined the regions: (A) $M_{vtx}>1.8\oplus P_{vtx}+10<15M_{vtx}$; (B) $M_{vtx}<1.8\oplus P_{vtx}>5\oplus P_{vtx}+10\geq 15M_{vtx}$; where $M_{vtx}(P_{vtx})$ is in units of GeV/c^2 (GeV/c); (C) all remaining events containing a SV. The boundaries of regions (A) and (B) are indicated in Figs. 2c and 2d, respectively, and all three regions are labelled in Fig. 2f. The b-tagged sample (subsample 1) was defined to comprise those events containing any vertex in region (A). For the remaining events containing any vertex in region (B), we examined the distribution of the impact parameter of the vector $P_{vtx}^{\rightarrow}$ with respect to the IP, δ_{vtx} (Fig. 3); according to the simulation true primary $c\bar{c}$ events dominate the population in the region $\delta_{vtx}<0.02$ cm. Therefore, we defined the c-tagged sample (subsample 2) to comprise those events in region (B) with $\delta_{vtx}<0.02$ cm.

Events containing no selected SV were then examined. For such events the distribution of N_{sig}, the number of

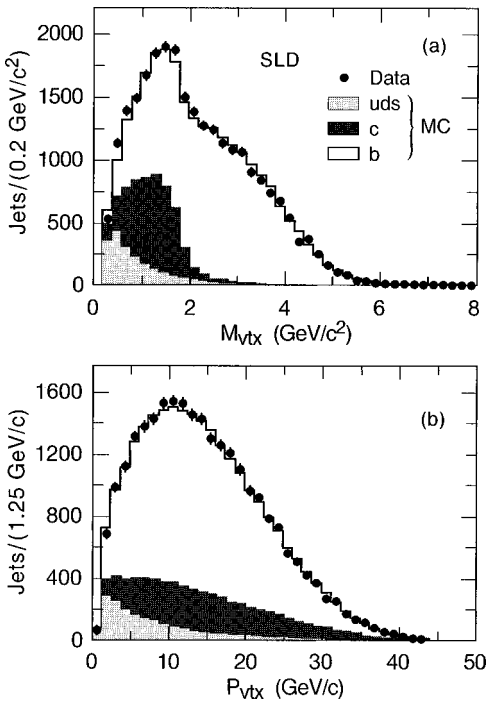

FIG. 1. The distributions of (a) the vertex mass, M_{vtx}, and (b) the vertex momentum, P_{vtx}, in our data sample (points); the simulated distributions are shown as a histogram in which the contributions from events of different primary quark flavor are indicated.

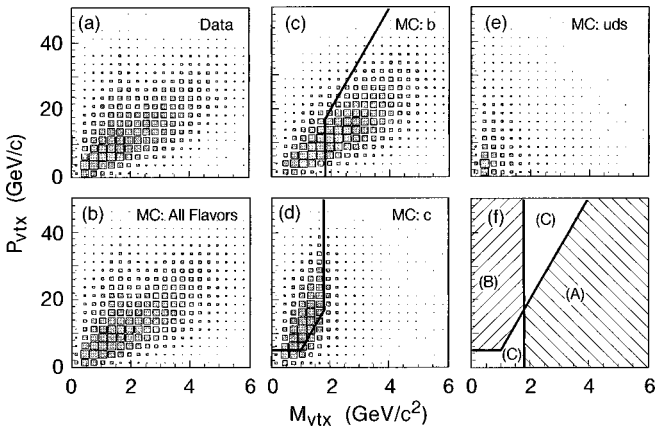

FIG. 2. The two-dimensional distribution of vertex momentum P_{vtx} vs vertex mass M_{vtx} (see text). (a) Data; (b) all-flavors simulation; (c) $b\bar{b}$ event simulation; (d) $c\bar{c}$ event simulation; (e) $q_l\bar{q}_l$ simulation. In (f) the regions used for b-tagging (A), c-tagging (B) and no-tagging (C) are indicated (see text).

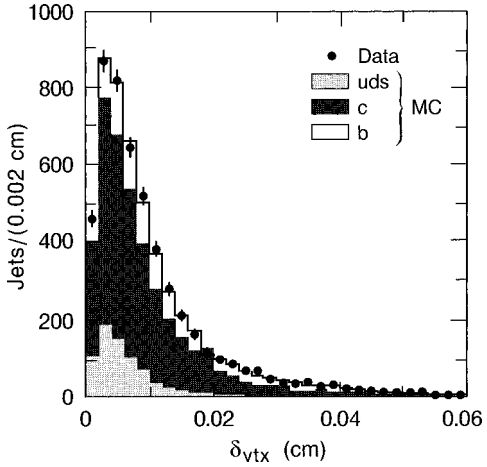

FIG. 3. The distribution of vertex impact parameter, δ_{vtx}, for events containing vertices in region (B): data (points); the simulated distribution is shown as a histogram in which the contributions from events of different primary quark flavor are indicated.

tracks per event that miss the IP by $d>2\sigma_d$, is shown in Fig. 4. The *uds*-tagged sample (subsample 3) was defined to comprise those events with $N_{\rm sig}=0$. All events not assigned to subsamples 1, 2 or 3 were defined to comprise the untagged sample (subsample 4). Using the simulation, we estimated that the efficiencies ε^{ji} for selecting events (after acceptance cuts) of type i ($i=b,c,uds,$) into subsample j ($1\leqslant j\leqslant 4$), and the fractions Π^{ji} of events of type i in subsample j, are $(\varepsilon,\Pi)^{1b}=(61.5\pm0.1\%,95.5\pm0.1\%)$, $(\varepsilon,\Pi)^{2c}=(19.1\pm0.1\%,64.4\pm0.3\%)$ and $(\varepsilon,\Pi)^{3uds}=(56.4\pm0.1\%,90.6\pm0.1\%)$. The composition of the untagged sample (subsample 4) was estimated to be $\Pi^{4uds}=59.3\pm0.1\%$, $\Pi^{4c}=24.1\pm0.1\%$ and $\Pi^{4b}=16.6\pm0.1\%$. The errors on these values are discussed in Sec. V.

IV. JET FINDING

For the study of flavor-independence, the jet structure of events was reconstructed in turn using six iterative clustering

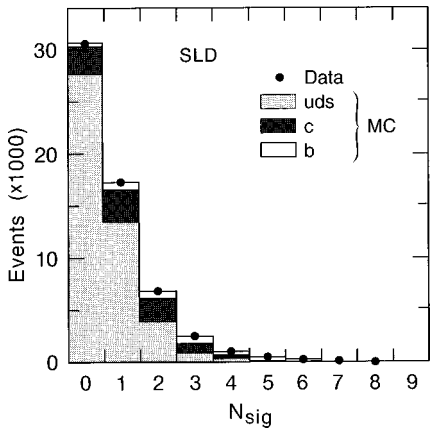

FIG. 4. The distribution of the number of tracks per event that miss the IP by at least 2σ in terms of their impact parameter in the plane normal to the beamline, in events that contain no reconstructed vertex (see text); data (points). The simulated distribution is shown as a histogram in which the contributions from events of different primary quark flavor are indicated.

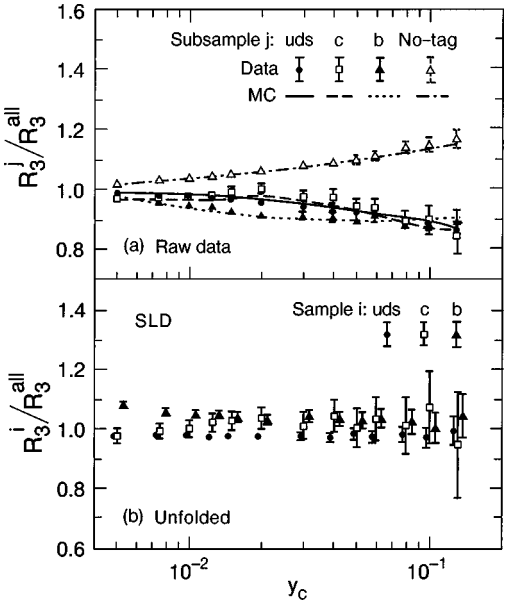

FIG. 5. (a) The raw measured ratios R_3^j/R_3^{all}, $1\leqslant j\leqslant 4$, vs y_c for the 4 subsamples (see text); data (points with error bars), and simulation (lines joining values at the same y_c values as the data). (b) The unfolded ratios R_3^i/R_3^{all}, $i=b$, c, *uds*, vs y_c for the 3 primary event flavor groups. Only statistical errors are shown. In (b) points corresponding to a common y_c value have been displaced horizontally for clarity.

algorithms. We used the ''E,'' ''E0,'' ''P,'' and ''P0'' variations of the JADE algorithm, as well as the ''Durham'' (''D'') and ''Geneva'' (''G'') algorithms [26]. In each case, events were divided into two categories: those containing (i) two jets, and (ii) three or more jets. The fraction of the event sample in category (ii) was defined as the 3-jet rate R_3. This quantity is infrared- and collinear-safe and has been calculated to $\mathcal{O}(\alpha_s^2)$ in perturbative QCD [26,27]. For each algorithm, we repeated the subsequent analysis successively across a range of values of the normalized jet-jet invariant-mass parameter y_c, $0.005\leqslant y_c\leqslant 0.12$. The ensemble of results from the different y_c values was used to cross-check the consistency of the method. In the final stage an ''optimal'' y_c value was chosen for each algorithm so as to minimize the overall error on the analysis, and the spread in results over the algorithms was used to assign an additional uncertainty (Sec. VII).

Each of the six jet-finding algorithms was applied to each tagged-event subsample j, $1\leqslant j\leqslant 3$. (Sec. III), as well as to the global sample of all accepted events (''all''). For each algorithm the 3-jet rate in each subsample was calculated, and the ratios R_3^j/R_3^{all}, in which many systematic errors should cancel, were then derived. As an example the R_3^j/R_3^{all} are shown as a function of y_c for the JADE E0 algorithm in Fig. 5a. The results of the corresponding analysis applied to the simulated event sample are also shown; the simulation reproduces the data. Similar results were obtained for the other jet algorithms (not shown).

For each algorithm and y_c value, the R_3^i for each of the i quark types ($i=b,c,uds$) was extracted from a simultaneous maximum likelihood fit to n_2^j and n_3^j, the number of 2-jet

and 3-jet events, respectively, in the flavor-tagged subsample $(1 \leqslant j \leqslant 3)$, using the relations

$$n_2^j = \sum_{i=uds,c,b} (\varepsilon^{ji}_{(2\to 2)}(1-R_3^i) + \varepsilon^{ji}_{(3\to 2)} R_3^i) f^i N$$

$$n_3^j = \sum_{i=uds,c,b} (\varepsilon^{ji}_{(3\to 3)} R_3^i + \varepsilon^{ji}_{(2\to 3)}(1-R_3^i)) f^i N. \tag{1}$$

Here N is the total number of events after correction for the event selection efficiency and f^i is the standard model fractional hadronic width for Z^0 decays to quark type i. The y_c-dependent 3×3 matrices $\varepsilon^{ji}_{(2\to 2)}$ and $\varepsilon^{ji}_{(3\to 3)}$ are the efficiencies for an event of type i, with 2- or 3-jets at the parton level, to pass all cuts and enter subsample j as a 2- or 3-jet event, respectively. Similarly, the 3×3 matrices $\varepsilon^{ji}_{(2\to 3)}$ and $\varepsilon^{ji}_{(3\to 2)}$ are the efficiencies for an event of type i, with 2- or 3-jets at the parton level, to pass all cuts and enter subsample j as a 3- or 2-jet event, respectively. These matrices were calculated from the Monte Carlo simulation and the systematic errors on the values of the matrix elements are discussed in Sec. V and VI.

This formalism explicitly accounts for modifications of the parton-level 3-jet rate due to hadronization, detector effects, and flavor-tagging bias. The latter effect is evident, for the E0 algorithm, in Fig. 5(a), where it can be seen that the measured values of R_3^j/R_3^{all} are below unity for subsamples $j=1$, 2 and 3, implying that the flavor tags preferentially select 2-jet rather than 3-jet events. For example, at $y_c = 0.02$ the normalized difference in efficiencies for correctly tagging a 2-jet event and a 3-jet event of type i in subsample j are $\mathcal{B}^{1,b}=5.7\%$, $\mathcal{B}^{2,c}=14.5\%$, and $\mathcal{B}^{3,uds}=4.1\%$, where $\mathcal{B}^{ji} \equiv (\varepsilon^{ji}_{2\to 2} - \varepsilon^{ji}_{3\to 3})/\varepsilon^{ji}_{2\to 2}$; these biases are considerably smaller than those found in [10], which resulted from the kinematic signatures employed for flavor-tagging. It should be noted that, as a corollary, the untagged event sample, subsample 4, contains an excess of 3-jet events [Fig. 5(a)]. Similar results were obtained for the other jet algorithms (not shown).

Equations (1) were solved using 2- and 3-jet events defined in turn by each of the six jet algorithms to obtain the true 3-jet rates in $Z^0 \to q_l \overline{q_l}$, $c\overline{c}$ and $b\overline{b}$ events, R_3^{uds}, R_3^c and R_3^b, respectively. Redefining $R_3^{all} = \Sigma_{b,c,uds} f^i R_3^i$, the unfolded ratios R_3^{uds}/R_3^{all}, R_3^c/R_3^{all} and R_3^b/R_3^{all} are shown in Fig. 5(b) for comparison with the raw measured values shown in Fig. 5(a).

For the test of the flavor-independence of strong interactions, it is more convenient to consider the ratios of the 3-jet rates in heavy- and light-quark events, namely R_3^c/R_3^{uds} and R_3^b/R_3^{uds}. These were derived from the unfolded R_3^{uds}, R_3^c and R_3^b values, and the systematic errors on the ratios are considered in the next sections.

V. EXPERIMENTAL SYSTEMATIC ERRORS

We considered sources of experimental systematic uncertainty that potentially affect our measurements of R_3^c/R_3^{uds} and R_3^b/R_3^{uds}. These may be divided into uncertainties in modelling the detector and uncertainties on experimental measurements serving as input parameters to the underlying physics modelling. In each case the error was evaluated by varying the appropriate parameter in the Monte Carlo simulation, recalculating the matrices ε, performing a new fit of Eq. (1) to the data, rederiving values of R_3^c/R_3^{uds} and R_3^b/R_3^{uds}, and taking the respective difference in results relative to our standard procedure as the systematic uncertainty.

In the category of detector modelling uncertainty, we considered the charged-particle tracking efficiency of the detector, as well as the smearing applied to the simulated charged-particle impact parameters in order to make the distributions agree with the data. An extra tracking inefficiency of roughly 3.5% was applied in the simulation in order to make the average number of charged tracks used for flavor-tagging agree with the data. We repeated the analysis in turn without this efficiency correction, and with no impact-parameter smearing, in the simulation.

A large number of measured quantities relating to the production and decay of charm and bottom hadrons are used as input to our simulation. In $b\overline{b}$ events we have considered the uncertainties on: the average charged multiplicity of B-hadron decays, the B-hadron fragmentation function, the production rate of b-baryons, the B-meson and B-baryon lifetimes, the inclusive production rate of D^+ mesons in B-hadron decays, and the branching fraction for $Z^0 \to b\overline{b}$, f^b. In $c\overline{c}$ events we have considered the uncertainties on: the branching fraction f^c for $Z^0 \to c\overline{c}$, the charmed hadron fragmentation function, the inclusive production rate of D^+ mesons, and the charged multiplicity of charmed hadron decays. We also considered the rate of production of secondary $b\overline{b}$ and $c\overline{c}$ from gluon splitting in $q\overline{q}g$ events. The values of these quantities used in our simulation and the respective variations that we considered are listed in Table I.

Statistical errors resulting from the finite size of the Monte Carlo event sample were estimated by generating 1,000 toy Monte Carlo data sets of the same size as that used in our data correction procedure, evaluating the matrices ε [Eq. (1)] for each, unfolding the data, and calculating the r.m.s. deviation of the distributions of the resulting R_3^c/R_3^{uds} and R_3^b/R_3^{uds} values.

As an example, for the E0 algorithm at $y_c = 0.02$, the errors on R_3^c/R_3^{uds} and R_3^b/R_3^{uds} from the above sources are listed in Table I. The dominant physics contributions to $\delta R_3^b/R_3^{uds}$ result from limited knowledge of the average B-hadron decay multiplicity and the B-hadron fragmentation function. The uncertainties in f^c and in the charmed hadron fragmentation function produce the dominant variations in R_3^c/R_3^{uds}. Contributions from B-hadron lifetimes, the fraction of D^+ in B meson decays, b-baryon production rates, and the charm hadron decay multiplicity are relatively small.

For each jet algorithm and y_c value all of the errors were added in quadrature to obtain a total experimental systematic error on R_3^c/R_3^{uds} and R_3^b/R_3^{uds}. The choice of an optimal y_c value is discussed in Sec. VI, and the combination of results from the six jet algorithms is discussed in Sec. VII.

TABLE I. Compilation of the systematic errors for the E0 algorithm and $y_{cut}=0.02$. The first column shows the error source, the second column the central value used, and the third column the variation considered. The remaining columns show the corresponding errors on the values of R_3^c/R_3^{uds} and R_3^b/R_3^{uds}; ''+'' (''−'') denotes the error corresponding to the relevant positive (negative) parameter variation.

Source	Center Value	Variation	$\delta R_3^c/R_3^{uds}$ +	$\delta R_3^c/R_3^{uds}$ −	$\delta R_3^b/R_3^{uds}$ +	$\delta R_3^b/R_3^{uds}$ −
tracking efficiency	correction	off	0.0020		−0.0110	
2D imp. par. res.	smear	off	−0.0100		0.0080	
z track resolution	smear	off	0.0010		0.0120	
MC statistics	0.8M	-	0.0190	−0.0190	0.0091	−0.0091
B decay $\langle n_{ch}\rangle$	5.51 trks	±0.35 trks	−0.0030	−0.0026	0.0135	−0.0132
B fragm. $\langle x_b\rangle$	0.697	±0.008	<0.0001	0.0004	0.0172	−0.0191
B fragm. shape	Peterson	Bowler	0.0021		−0.0216	
B meson lifetime	1.56 ps	±0.05 ps	−0.0021	0.0022	−0.0011	0.0009
B baryon lifetime	1.10 ps	±0.08 ps	−0.0003	0.0003	<0.0001	−0.0000
B baryon prod.	7.6%	±3.2%	0.0014	−0.0016	0.0021	−0.0023
$B\to D^+ + X$ fraction	0.192	±0.05	0.0011	−0.0012	−0.0013	−0.0008
$Z^0\to b\bar{b}$: f^b	0.2156	±0.0017	0.0022	−0.0021	0.0014	−0.0014
$Z^0\to c\bar{c}$: f^c	0.172	±0.010	0.0272	−0.0294	0.0044	−0.0042
C fragm. $\langle x_c\rangle$	0.483	±0.008	0.0213	−0.0211	0.0002	−0.0002
C fragm. shape	Peterson	Bowler	0.0042		0.0006	
D^0 decay $\langle n_{ch}\rangle$	2.54 trks	±0.06 trks	0.0044	−0.0048	0.0006	−0.0006
D^+ decay $\langle n_{ch}\rangle$	2.48 trks	±0.06 trks	0.0069	−0.0074	0.0012	−0.0013
D_s decay $\langle n_{ch}\rangle$	2.62 trks	±0.31 trks	0.0039	−0.0040	−0.0004	0.0003
D^0 lifetime	0.418 ps	±0.004 ps	−0.0001	0.0001	−0.0002	0.0001
D^+ lifetime	1.054 ps	±0.015 ps	0.0001	−0.0001	−0.0001	0.0001
D_s lifetime	0.466 ps	±0.017 ps	0.0001	−0.0001	−0.0003	0.0003
$D^0\to K^0$ mult.	0.402	±0.059	0.0088	−0.0089	0.0026	−0.0026
$D^+\to K^0$ mult.	0.644	±0.078	0.0102	−0.0120	0.0027	−0.0027
$D_s\to K^0$ mult.	0.382	±0.057	0.0012	−0.0013	0.0003	−0.0003
$D^0\to$no π^0 fraction	0.370	±0.037	0.0069	−0.0075	0.0034	−0.0034
$D^+\to$no π^0 fraction	0.496	±0.050	0.0017	−0.0018	0.0029	−0.0029
$D_s\to$no π^0 fraction	0.348	±0.035	−0.0002	0.0001	−0.0003	0.0003
$c\bar{c}\to D^+ + X$ fraction	0.259	±0.028	0.0029	−0.0034	0.0001	−0.0002
$c\bar{c}\to D_s + X$ fraction	0.113	±0.037	−0.0025	0.0019	0.0002	−0.0002
$c\bar{c}\to \Lambda_c + X$ fraction	0.074	±0.029	−0.0051	0.0044	−0.0001	−0.0001
Λ_c decay $\langle n_{ch}\rangle$	2.79	±0.45 trks	0.0003	−0.0002	0.0024	−0.0024
Λ_c lifetime	0.216 ps	±0.011 ps	−0.0037	0.0011	−0.0006	0.0001
$g\to bb$ rate	0.31	±0.11%	0.0001	−0.0001	−0.0038	0.0039
$g\to cc$ rate	2.38	±0.48%	−0.0019	0.0020	−0.0015	0.0016
K^0 prodn.	0.658 trks	±0.050 trks	−0.0051	0.0045	−0.0061	0.0058
Λ prodn.	0.124 trks	±0.008 trks	−0.0007	0.0009	−0.0008	0.0009
Total Exp. Syst.			0.0440	−0.0480	0.0300	−0.0370
Q_0	1 GeV	$^{+1}_{-0.5}$ GeV	0.0074	−0.0027	0.0062	−0.0237
σ_q	0.39 GeV	±0.04 GeV	0.0042	−0.0008	0.0015	0.0012
hadronization model	JETSET 7.4	HERWIG 5.9	0.0123		−0.0383	
Total Hadronization			0.0150	−0.0028	0.0065	−0.0450

VI. THEORETICAL UNCERTAINTIES AND TRANSLATION TO α_s RATIOS

We considered sources of theoretical uncertainty that potentially affect our measurements. The ratios R_3^c/R_3^{uds} and R_3^b/R_3^{uds} derived in Sec. IV were implicitly corrected for the effects of hadronization and we have estimated the uncertainty in this correction. Furthermore, the $\geqslant$3-jet rate in heavy-quark events is modified relative to that in light-quark events by the effect of the non-zero quark mass. This effect needs to be taken into account in the translation between the jet-rate ratios and the corresponding ratios of strong couplings $\alpha_s^c/\alpha_s^{uds}$ and $\alpha_s^b/\alpha_s^{uds}$. We have used $O(\alpha_s^2)$ calcula-

tions to perform the mass-dependent translation, and have estimated the related uncertainties due to the value of the *b*-quark mass, as well as higher-order perturbative QCD contributions.

A. Hadronization uncertainties

The intrinsically non-perturbative process by which quarks and gluons fragment into the observed final-state hadrons cannot currently be calculated in QCD. Phenomenological models of hadronization have been developed over the past few decades and have been implemented in Monte Carlo event-generator programs to facilitate comparison with experimental data. We have used the models implemented in the JETSET 7.4 and HERWIG 5.9 [28] programs to study hadronization effects; these models have been extensively studied and tuned to provide a good description of detailed properties of hadronic final states in e^+e^- annihilation; for a review of studies at the Z^0 resonance, see [29]. Our standard simulation based on JETSET 7.4 was used to evaluate the efficiency and purity of the event-flavor tagging, as described in Sec. IV, as well as for the study of experimental systematic errors described in Sec. V.

We investigated hadronization uncertainties by calculating from the Monte Carlo-generated event sample, the ratios:

$$r_i \equiv \left(\frac{R_3^i}{R_3^{uds}}\right)_{parton} \Bigg/ \left(\frac{R_3^i}{R_3^{uds}}\right)_{hadron}$$

where $i=c$ or b, *parton* refers to the calculation of the quantity in brackets at the parton-level and hadron refers to the corresponding hadron-level calculation using stable final-state particles. We recalculated these ratios by changing in turn the parameters Q_0 and σ_q in the JETSET program[3] and generating 1-million-event samples. We also recalculated these ratios by using the HERWIG 5.9 program with default parameter settings. For each variation we evaluated the fractional deviation Δr_i with respect to the standard value:

$$\Delta r_i = \frac{(r_i' - r_i)}{r_i},$$

and the corresponding deviations on R_3^i/R_3^{uds}. As an example, for the E0 algorithm and $y_c=0.02$, the deviations are listed in Table I. The deviations were added in quadrature to define the systematic error on R_3^i/R_3^{uds} due to hadronization uncertainties.

[3] Q_0 (GeV) controls the minimum virtual mass allowed for partons in the parton shower; we considered a variation around the central value, 1.0, of $^{+1.0}_{-0.5}$. σ_q (GeV/c) is the width of the Gaussian distribution used to assign transverse momentum, with respect to the color field, to quarks and antiquarks produced in the fragmentation process; we considered a variation around the central value, 0.39, of ± 0.04.

B. Choice of y_c values

For each jet algorithm and y_c value, the statistical and experimental systematic errors and hadronization uncertainty on each R_3^i/R_3^{uds} were added in quadrature. No strong dependence of this combined error on y_c was observed [30], but an ''optimal'' y_c value for each algorithm was then identified that corresponded with the smallest error. In the case of the E and G algorithms slightly larger y_c values were chosen so as to ensure that the $O(\alpha_s^2)$ calculations for massive quarks were reliable [31]. The chosen y_c value for each algorithm is listed in Table II, together with the corresponding values of the ratios R_3^c/R_3^{uds} and R_3^b/R_3^{uds}, as well as the statistical and experimental-systematic errors and hadronization uncertainties.

C. Translation to α_s ratios

The test of the flavor-independence of strong interactions can be expressed in terms of the ratios $\alpha_s^i/\alpha_s^{uds}$ ($i=c$ or b). Recalling that with our definition, R_3 is the rate of production of 3 or more jets, $\alpha_s^i/\alpha_s^{uds}$ can be derived from the respective measured ratio R_3^i/R_3^{uds} using the next-to-leading-order perturbative QCD calculation:

$$\frac{R_3^i}{R_3^{uds}} = \frac{A^i\overline{\alpha_s^i} + [B^i + C^i](\overline{\alpha_s^i})^2 + O((\overline{\alpha_s^i})^3)}{A^{uds}\overline{\alpha_s^{uds}} + [B^{uds} + C^{uds}](\overline{\alpha_s^{uds}})^2 + O((\overline{\alpha_s^{uds}})^3)}, \quad (2)$$

where $\overline{\alpha_s} = \alpha_s/2\pi$, and the coefficients A, B and C represent, respectively, the leading-order (LO) perturbative QCD coefficient for the 3-jet rate, the next-to-leading-order (NLO) coefficient for this rate, and the leading-order coefficient for the 4-jet rate. Next-to-leading-order contributions to the 4-jet rate, and contributions from $\geqslant$5-jet rates, are represented by the terms of $O(\alpha_s^3)$. These coefficients depend implicitly upon the jet algorithm as well as on the scaled-invariant-mass-squared jet resolution parameter y_c; for clarity these dependences have been omitted from the notation. For massless quarks calculations of the coefficients A, B and C have been available for many years [26,27].

For many observables at the Z^0 pole, the quark mass appears in terms proportional to the ratio m_q^2/M_Z^2, and the effects of non-zero quark mass can be neglected. For the jet rates, however, mass effects can enter via terms proportional to $m_q^2/(y_c M_Z^2)$. For b-quarks these terms can contribute at the O(5%) level for typical values of y_c used in jet clustering. Therefore, the $\geqslant$3-jet rate in heavy-quark events is expected to be modified relative to that in light-quark events both by the diminished phase-space for gluon emission due to the quark mass, as well as by kinematic effects in the definition of the jet clustering schemes. Such mass effects for jet rates have very recently been calculated [12,13] at NLO in perturbative QCD,[4] and the quark-mass dependence can be expressed in terms of the running mass $m_b(M_{Z^0})$. The

[4] In our previous study [11] only the relevant tree-level calculations for 3-jet and 4-jet final-states were available.

TABLE II. R_3^i/R_3^{uds} and $\alpha_s^i/\alpha_s^{uds}$ values and errors.

Algorithm	E	E0	P	P0	D	G	
y_c	0.040	0.020	0.020	0.015	0.010	0.080	
			R_3^c/R_3^{uds}				
central val.	1.043	1.066	1.004	1.058	1.038	1.040	
stat.	0.064	0.046	0.046	0.040	0.062	0.086	
exp. syst.	$^{+0.065}_{-0.075}$	$^{+0.044}_{-0.048}$	$^{+0.046}_{-0.046}$	$^{+0.039}_{-0.039}$	$^{+0.062}_{-0.067}$	$^{+0.074}_{-0.085}$	
hadronization	$^{+0.012}_{-0.001}$	$^{+0.015}_{-0.003}$	$^{+0.014}_{-0.004}$	$^{+0.015}_{-0.003}$	$^{+0.006}_{-0.003}$	$^{+0.008}_{-0.004}$	
total.	$^{+0.092}_{-0.099}$	$^{+0.065}_{-0.067}$	$^{+0.067}_{-0.065}$	$^{+0.058}_{-0.056}$	$^{+0.088}_{-0.091}$	$^{+0.114}_{-0.121}$	
			$\alpha_s^c/\alpha_s^{uds}$				rms
central val.	1.031	1.054	1.004	1.052	1.032	1.035	0.017
stat.	0.046	0.037	0.041	0.035	0.051	0.074	
exp. syst.	$^{+0.047}_{-0.054}$	$^{+0.036}_{-0.039}$	$^{+0.041}_{-0.041}$	$^{+0.035}_{-0.035}$	$^{+0.051}_{-0.055}$	$^{+0.064}_{-0.073}$	
hadronization	$^{+0.009}_{-0.001}$	$^{+0.012}_{-0.002}$	$^{+0.012}_{-0.001}$	$^{+0.013}_{-0.003}$	$^{+0.005}_{-0.002}$	$^{+0.007}_{-0.001}$	
translation	$^{+0.001}_{-0.002}$	$^{+0.005}_{-0.006}$	<0.001	± 0.008	$^{+0.003}_{-0.005}$	$^{+0.004}_{-0.006}$	
			R_3^b/R_3^{uds}				
central val.	1.050	1.054	1.048	1.055	0.964	0.995	
stat.	0.026	0.019	0.019	0.017	0.023	0.032	
exp. syst.	$^{+0.038}_{-0.042}$	$^{+0.030}_{-0.037}$	$^{+0.027}_{-0.037}$	$^{+0.028}_{-0.035}$	$^{+0.038}_{-0.041}$	$^{+0.035}_{-0.036}$	
hadronization	$^{+0.011}_{-0.046}$	$^{+0.007}_{-0.045}$	$^{+0.002}_{-0.026}$	$^{+0.007}_{-0.037}$	$^{+0.001}_{-0.006}$	$^{+0.020}_{-0.008}$	
total.	$^{+0.047}_{-0.067}$	$^{+0.036}_{-0.061}$	$^{+0.033}_{-0.049}$	$^{+0.033}_{-0.054}$	$^{+0.044}_{-0.047}$	$^{+0.051}_{-0.049}$	
			$\alpha_s^b/\alpha_s^{uds}$				rms
central val.	0.989	0.995	1.018	1.014	1.009	0.993	0.011
stat.	0.018	0.015	0.017	0.015	0.021	0.027	
exp. syst.	$^{+0.026}_{-0.029}$	$^{+0.023}_{-0.028}$	$^{+0.023}_{-0.032}$	$^{+0.024}_{-0.030}$	$^{+0.034}_{-0.036}$	$^{+0.030}_{-0.031}$	
hadronization	$^{+0.008}_{-0.032}$	$^{+0.005}_{-0.034}$	$^{+0.002}_{-0.022}$	$^{+0.006}_{-0.032}$	$^{+0.001}_{-0.005}$	$^{+0.017}_{-0.007}$	
translation	$^{+0.016}_{-0.015}$	$^{+0.013}_{-0.015}$	$^{+0.011}_{-0.014}$	$^{+0.017}_{-0.018}$	± 0.012	$^{+0.008}_{-0.009}$	

Aachen group has evaluated [31] the terms A^b, B^b and C^b for massive *b*-quarks at our preferred values of y_c; these are listed in Table III.

For illustration, the measured ratios R_3^c/R_3^{uds} and R_3^b/R_3^{uds}, are shown in Fig. 6(a). R_3^b/R_3^{uds} lies above unity for the E, E0, P and P0 algorithms, and below unity for the D and G algorithms; note that all six data points are highly correlated with each other, so that the differences between algorithms are more significant than naively implied by the statistical errors displayed. For comparison, the corresponding QCD calculations of R_3^b/R_3^{uds} are also shown in Fig. 6(a), under the *assumption* of a flavor-independent strong coupling with an input value of $\alpha_s(M_Z^2)=0.118$, for $m_b(M_{Z^0})=3.0\pm 0.5\ \mathrm{GeV}/c^2$. Under this assumption, the calculations are in good agreement with the data, and the data clearly demonstrate the effects of the non-zero *b*-quark mass, which are larger than the statistical error. For the translation from R_3^b/R_3^{uds} to $\alpha_s^b/\alpha_s^{uds}$, we used a value of the running *b*-quark mass $m_b(M_{Z^0})=3.0\ \mathrm{GeV}/c^2$.

For *c*-quarks, mass effects are expected to be O(1%) or less [31], which is much smaller than our statistical error of roughly 4% on R_3^c/R_3^{uds}. The effects of non-zero *c*-quark mass, and of the light-quark masses, will hence be neglected here. We used values of A^{uds}, B^{uds} and C^{uds} from Ref. [26].

Equations (2) were solved to obtain the ratios $\alpha_s^c/\alpha_s^{uds}$ and $\alpha_s^b/\alpha_s^{uds}$ for each jet algorithm. These ratios are listed in Table II, together with the corresponding statistical and experimental systematic errors, and the hadronization uncertainties. We then evaluated sources of uncertainty in this translation procedure. From an operational point of view, these affect the values of the coefficients *A*, *B* and *C* used for the translation. For each variation considered, the relevant *A*, *B* or *C* were reevaluated, the ratios $\alpha_s^i/\alpha_s^{uds}$ were rederived, and the deviation with respect to the central value was assigned as a systematic uncertainty.

We considered a variation of $\pm 0.5\ \mathrm{GeV}/c^2$ about the central value of the running *b*-quark mass $m_b(M_{Z^0})=3.0\ \mathrm{GeV}/c^2$. This corresponds to the range $3.62<m_b(m_b)<5.06\ \mathrm{GeV}/c^2$ and covers generously the values [13] determined from the Υ system using QCD sum rules, $4.13\pm 0.06\ \mathrm{GeV}/c^2$, as well as using lattice QCD, $4.15\pm 0.20\ \mathrm{GeV}/c^2$. It is also consistent with the recent DELPHI

TABLE III. The coefficients A^b, B^b, C^b for the next-to-leading-order calculation for massive quarks. The numbers in parentheses represent the estimated numerical precision. Theoretical uncertainties in the computation of the B^b coefficients derive from the ''slicing parameter'' used to isolate singular regions of phase space, as well as from the conversion to the $\overline{\text{MS}}$ quark mass parameter Effects from higher-order perturbative QCD contributions are discussed in the text.

		A^b for $m_b(M_{Z^0})$ (GeV/c^2)=			B^b for $m_b(M_{Z^0})$ (GeV/c^2)=		
Algorithm	y_c	2.5	3	3.5	2.5	3	3.5
E	0.040	14.392(1)	14.459(1)	14.543(1)	443(4)	466(4)	487(4)
E0	0.020	24.850(2)	25.024(2)	25.231(2)	277(4)	291(4)	310(4)
P	0.020	24.850(2)	25.024(2)	25.231(2)	63(4)	67(4)	75(4)
P0	0.015	30.054(2)	30.315(2)	30.631(2)	2(4)	14(4)	29(4)
D	0.010	15.355(2)	15.213(2)	15.060(2)	105(4)	102(4)	99(4)
G	0.080	11.493(1)	11.435(1)	11.365(1)	61(4)	58(4)	57(4)

		C^b for $m_b(M_{Z^0})$ (GeV/c^2)=		
Algorithm	y_c	2.5	3	3.5
E	0.040	27.91(1)	28.27(1)	28.71(1)
E0	0.020	125.39(7)	127.34(7)	129.55(8)
P	0.020	125.39(7)	127.34(7)	129.55(8)
P0	0.015	202.8(1)	206.1(1)	209.4(1)
D	0.010	84.30(6)	82.83(6)	81.19(6)
G	0.080	65.55(4)	64.60(3)	63.56(3)

measurement of the running mass: $m_b(M_{Z^0}) = 2.67 \pm 0.25(\text{stat}) \pm 0.34(\text{frag}) \pm 0.27(\text{theo}) \text{GeV}/c^2$ [5]. The numerical accuracy on the coefficients *A*, *B*, and *C* is in all cases negligibly small on the scale of the experimental statistical errors.

We considered the effects of the uncalculated higher-order terms in Eq. (2). In these ratios, the effects of such higher-order contributions will tend to cancel. Nevertheless, we have attempted to evaluate the residual uncertainty due to these contributions. We first considered 3-jet contributions and varied the NLO coefficient *B*; for each jet algorithm we varied simultaneously the renormalization scale μ and α_s^{uds} in the ranges allowed by fits to the flavor-inclusive differential 2-jet rate [15].[5] In addition, we considered NLO contributions to the 4-jet rate. Although these enter formally at $O(\alpha_s^3)$ in Eq. (2), operationally they may be estimated by variation of the LO coefficient C^i. Since the 4-jet rate has been calculated recently complete at NLO for massless quarks [32], these terms can be estimated reliably. For our jet algorithms and y_c values, Dixon has evaluated the LO and NLO 4-jet contributions [33]. Based on these calculations, we varied the coefficient *C* by $\pm 100\%$. For each jet algorithm, at the chosen y_c value, the measured contribution to R_3 from $\geqslant$5-jet states was smaller than 1% and the corresponding $O(\alpha_s^3)$ contributions to Eq. (2) were neglected.

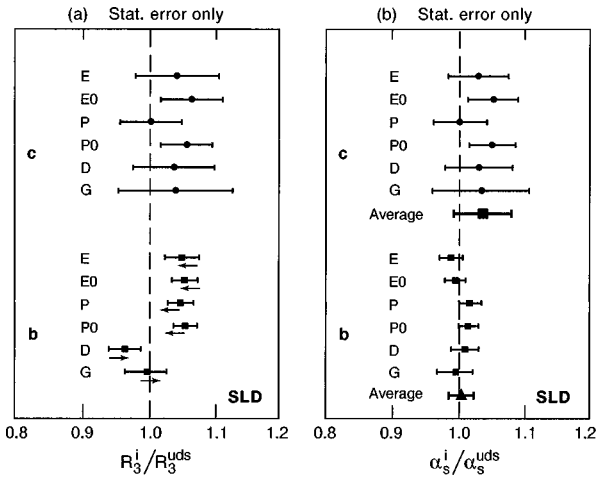

FIG. 6. (a) The measured ratios R_3^i/R_3^{uds} and (b) the corresponding translated ratios α_s^i/α^{uds} $(i=c,b)$. The arrows in (a) indicate the range of the theoretical prediction described in the text for values of the *b*-quark mass in the range $2.5 \leqslant m_b(M_{Z^0}) \leqslant 3.5$ GeV/c^2, with the arrow pointing towards the lower mass value. In (b) the weighted average over the six algorithms is also shown. In all cases only statistical error bars are displayed.

These uncertainties are summarized in Table IV. The deviations for each variation considered were added in quadrature to define a total translation uncertainty on $\alpha_s^c/\alpha_s^{uds}$ and $\alpha_s^b/\alpha_s^{uds}$, listed in Table II.

VII. COMPARISON OF α_s RATIOS

The $\alpha_s^c/\alpha_s^{uds}$ and $\alpha_s^b/\alpha_s^{uds}$ ratios are summarized in Fig. 6b. It can be seen that the ratios determined using the differ-

[5]Heavy-quark mass and possible flavor-dependent effects are negligible on the scale of the large errors considered on α_s^{uds} for this purpose.

TABLE IV. Summary of translation uncertainties on the α_s ratios for each algorithm; ''+'' (''−'') denotes the error corresponding to the relevant positive (negative) parameter variation.

			$\delta\alpha_s^c/\alpha_s^{uds}$		$\delta\alpha_s^b/\alpha_s^{uds}$	
Source	Center	Variation	+	−	+	−
			E-algo ($y_c=0.04$)			
$m_b(M_Z)$	3.0 GeV	±0.5	0.000	0.000	−0.014	0.015
μ, α_s dep.			−0.002	0.001	0.006	−0.006
⩾ 4jet contrib.	C	$\pm C$	<0.001	<0.001	−0.001	0.001
Total			0.001	−0.002	0.016	−0.015
			E0-algo ($y_c=0.02$)			
$m_b(M_Z)$	3.0 GeV	±0.5	0.000	0.000	−0.014	0.012
μ, α_s dep.			−0.005	0.004	0.005	−0.005
⩾ 4jet contrib.	C	$\pm C$	−0.002	0.003	−0.001	0.002
Total			0.005	−0.006	0.013	−0.015
			P-algo ($y_c=0.02$)			
$m_b(M_Z)$	3.0 GeV	±0.5	0.000	0.000	−0.012	0.009
μ, α_s dep.			<0.001	<0.001	−0.002	0.002
⩾ 4jet contrib.	C	$\pm C$	<0.001	<0.001	−0.005	0.007
Total			<0.001	<0.001	0.011	−0.014
			P0-algo ($y_c=0.015$)			
$m_b(M_Z)$	3.0 GeV	±0.5	0.000	0.000	−0.017	0.015
μ, α_s dep.			−0.007	0.005	−0.001	<0.000
⩾ 4jet contrib.	C	$\pm C$	−0.004	0.006	−0.006	0.008
Total			0.008	−0.008	0.017	−0.018
			D-algo ($y_c=0.010$)			
$m_b(M_Z)$	3.0 GeV	±0.5	0.000	0.000	0.011	−0.010
μ, α_s dep.			−0.005	0.002	−0.005	0.003
⩾ 4jet contrib.	C	$\pm C$	−0.002	0.002	−0.003	0.003
Total			0.003	−0.005	0.012	−0.012
			G-algo ($y_c=0.08$)			
$m_b(M_Z)$	3.0 GeV	±0.5	0.000	0.000	0.010	−0.009
μ, α_s dep.			−0.005	0.003	0.005	−0.003
⩾ 4jet contrib.	C	$\pm C$	−0.002	0.003	0.001	−0.001
Total			0.004	−0.006	0.008	−0.009

ent jet algorithms are in good agreement with one another.

For each jet algorithm n, the statistical and experimental systematic errors were added in quadrature with the hadronization and translation uncertainties (Table II) to define a total error σ_n^i on $\alpha_s^i/\alpha_s^{uds}$ ($i=c$ or b). For each flavor a single value of $\alpha_s^i/\alpha_s^{uds}$ was then defined by taking the weighted average of the results over the six jet algorithms:

$$\alpha_s^i/\alpha_s^{uds}=\sum_n w_n^i(\alpha_s^i/\alpha_s^{uds})_n, \tag{3}$$

where w_n^i is the weight for each algorithm:

$$w_n^i=\frac{1/\sigma_n^{i^2}}{\Sigma_n 1/\sigma_n^{i^2}}. \tag{4}$$

The average statistical and experimental systematic errors were each computed from:

$$\overline{\sigma^i}=\sqrt{\sum_{nm} E_{nm}^i w_n^i w_m^i}, \tag{5}$$

where E^i is the 6×6 covariant matrix with elements:

$$E_{nm}^i=\sigma_n^i\sigma_m^i \tag{6}$$

and 100% correlation was conservatively assumed among algorithms. The average translation and hadronization uncertainties were calculated in a similar fashion. We then calculated the r.m.s. deviation on $\alpha_s^c/\alpha_s^{uds}$ and $\alpha_s^b/\alpha_s^{uds}$, shown in Table II, and assigned this scatter between the results from different algorithms as an additional theoretical uncertainty. The average translation and hadronization uncertainties were added in quadrature together with the r.m.s. deviation to define the total theoretical uncertainty.

We obtained:

$$\alpha_s^c/\alpha_s^{uds}=1.036\pm 0.043(\text{stat})^{+0.041}_{-0.045}(\text{syst})^{+0.020}_{-0.018}(\text{theory}),$$

$$\alpha_s^b/\alpha_s^{uds} = 1.004 \pm 0.018(\text{stat})^{+0.026}_{-0.031}(\text{syst})^{+0.018}_{-0.029}(\text{theory}).$$

The theoretical uncertainties are only slightly smaller than the respective experimental systematic errors, and comprise roughly equal contributions from the hadronization and translation uncertainties, as well as from the rms deviation over the six jet algorithms.

VIII. CROSS-CHECKS

We performed a number of cross-checks on these results. First, we varied the event selection requirements. The thrust-axis containment cut was varied in the range $0.65 < |\cos\theta_T| < 0.75$, the minimum number of charged tracks required was increased from 7 to 8, and the total charged-track energy requirement was increased from 20 to 22 GeV. In each case results consistent with the standard selection were obtained.

Next, we included in the unfolding procedure [Eq. (1) and Sec. IV] the ''untagged'' event sample, subsample 4 (Sec. III), whose flavor composition is similar to the natural composition in flavor-inclusive Z^0 decay events, and repeated the analysis to derive new values of $\alpha_s^c/\alpha_s^{uds}$ and $\alpha_s^b/\alpha_s^{uds}$. In addition, we repeated the unfolding and, instead of fixing them to standard model values (Table I), allowed the $Z^0 \to c\bar{c}$ and $Z^0 \to b\bar{b}$ branching fractions to float in the fit of Eq. (1). In both cases results consistent with the standard procedure were obtained [30].

We also considered variations of the flavor-tagging scheme based on reconstructed secondary vertices. In each case we repeated the analysis described in Sec. IV–VII and derived new values of $\alpha_s^c/\alpha_s^{uds}$ and $\alpha_s^b/\alpha_s^{uds}$. Firstly, we used more efficient tags for primary $b\bar{b}$ and $c\bar{c}$ events. We applied the scheme described in Sec. III, but with a looser definition of region (*A*) to include vertices with $M_{vtx} > 1.8$ or $P_{vtx} + 10 < 15 M_{vtx}$. We also removed the cut on the vertex impact parameter, δ_{vtx}, used to define the *c*-tagged sample, and region (*B*) was redefined to comprise only events with $N_{sig} \geq 1$ and containing a SV with $P_{vtx} > 5 \oplus P_{vtx} + 10 > 15 M_{vtx}$. Second, we repeated this modified scheme, but increased the efficiency for light-quark tagging by requiring tracks that miss the IP by at least $3\sigma_d$ to be counted in N_{sig} for the definition of the *uds*-tagged sample. Third, we did not use vertex momentum information for the tag definitions; we used instead only vertex mass information to define region (*A*): $M_{vtx} > 1.8$, and Region (*B*): $M_{vtx} < 1.8$, with the *uds*-tagged sample defined as in Sec. IV. Finally, we tried a variation in which we used event hemispheres as a basis for flavor-tagging, rather than jets as defined in Sec. III; this tag is similar to that used in our recent study of the branching fraction for $Z^0 \to b\bar{b}$ [34]. In all cases results statistically consistent with our standard analysis were obtained [30].

We also performed an analysis using a similar flavor-tagging technique to that reported in our previous publication [11]. We counted the number of tracks per event, N_{sig}, that miss the IP by $d > 3\sigma_d$. This distribution is shown in Fig. 7; the data are well described by our Monte Carlo simulation. For the simulation, the contributions of events of different quark flavors are shown separately. The left most bin contains predominantly events containing primary *u*, *d*, or *s* quarks, while the right most bins contain a pure sample of events containing primary *b* quarks. The event sample was divided accordingly into five subsamples according to the number of ''significant'' tracks: (i) $N_{sig} = 0$, (ii) $N_{sig} = 1$, (iii) $N_{sig} = 2$, (iv) $N_{sig} = 3$, and (v) $N_{sig} \geq 4$. A similar formalism to that defined by Eq. (1) was applied using 5×3 matrices ε and yielded values of R_3^{uds}/R_3^{all}, R_3^c/R_3^{all} and R_3^b/R_3^{all} consistent with those obtained in Secs. IV and V, but with larger statistical and systematic errors. Furthermore, we also ap-

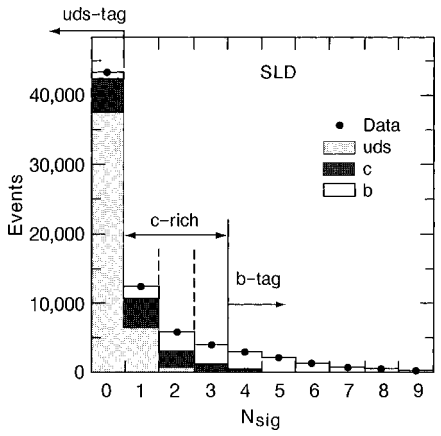

FIG. 7. The distribution of the number of tracks that miss the IP by at least 3σ in terms of their impact parameter in the plane normal to the beamline (see text): data (points); the simulated distribution is shown as a histogram in which the contributions from events of different primary quark flavor are indicated.

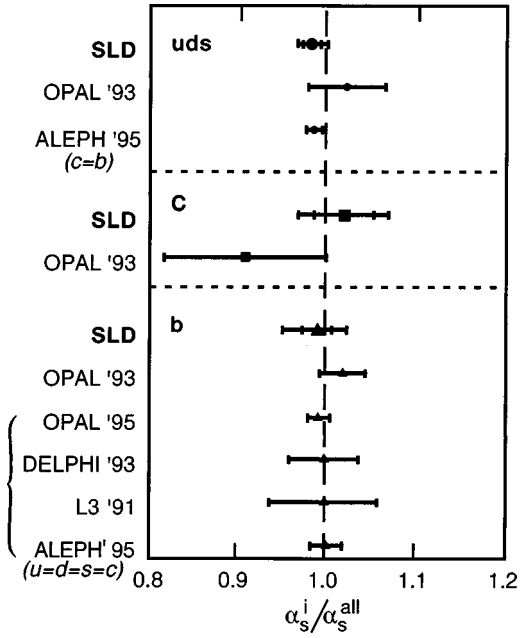

FIG. 8. Summary of measurements of $\alpha_s^i/\alpha_s^{all}$ ($i = uds$, *c* or *b*) from experiments at the Z^0 resonance. We derived the ALEPH $\alpha_s^{uds}/\alpha_s^{all}$ value from their measured value of $\alpha_s^{uds}/\alpha_s^{bc}$, as well as the four bracketed LEP values of $\alpha_s^b/\alpha_s^{all}$ from the measured values of $\alpha_s^b/\alpha_s^{udsc}$, by assuming $\alpha_s^{all} = \Sigma_{uds,c,b} f^i \alpha_s^i$, where f^i is the standard model branching fraction for Z^0 decays to quark flavor *i*.

plied a simpler version of this technique in which subsamples (ii), (iii) and (iv) were combined into a single c-tagged sample and a 3×3 flavor unfolding was performed. Again, this yielded values of R_3^{uds}/R_3^{all}, R_3^c/R_3^{all} and R_3^b/R_3^{all} consistent with those obtained in Secs. IV and V, but with larger statistical and systematic errors [30].

IX. SUMMARY AND DISCUSSION

We have used hadron lifetime and mass information to separate hadronic Z^0 decays into tagged $b\bar{b}$, $c\bar{c}$ and light-quark event samples with high efficiency and purity, and small bias against events containing hard gluon radiation. From a comparison of the rates of multijet events in these samples, we obtained

$$\alpha_s^c/\alpha_s^{uds} = 1.036 \pm 0.043(\text{stat})^{+0.041}_{-0.045}(\text{syst})^{+0.020}_{-0.018}(\text{theory}),$$

$$\alpha_s^b/\alpha_s^{uds} = 1.004 \pm 0.018(\text{stat})^{+0.026}_{-0.031}(\text{syst})^{+0.018}_{-0.029}(\text{theory}).$$

We find that the strong coupling is independent of quark flavor within our sensitivity.

For comparison with our previous result and with other experiments, one can discuss the test of flavor-independence in terms of the ratios $\alpha_s^{uds}/\alpha_s^{all}$, $\alpha_s^c/\alpha_s^{all}$ and $\alpha_s^b/\alpha_s^{all}$, although these quantities, by construction, are not independent of each another. We performed a similar analysis to that described in Secs. VI and VII using, instead of R_3^c/R_3^{uds} and R_3^b/R_3^{uds}, our measured values of R_3^{uds}/R_3^{all}, R_3^c/R_3^{all} and R_3^b/R_3^{all} (Sec. IV) as a starting point. We obtained:

$$\alpha_s^{uds}/\alpha_s^{all} = 0.987 \pm 0.010(\text{stat})^{+0.012}_{-0.010}(\text{syst})^{+0.009}_{-0.008}(\text{theory}),$$

$$\alpha_s^c/\alpha_s^{all} = 1.023 \pm 0.034(\text{stat})^{+0.032}_{-0.036}(\text{syst})^{+0.018}_{-0.014}(\text{theory}),$$

$$\alpha_s^b/\alpha_s^{all} = 0.993 \pm 0.016(\text{stat})^{+0.020}_{-0.023}(\text{syst})^{+0.019}_{-0.027}(\text{theory}).$$

These results are consistent with, and supersede, our previous measurements [11], and are substantially more precise; they are also consistent with measurements performed at LEP using different flavor-tagging techniques [5,8,9,10]. A summary of these results is given in Fig. 8. Our comprehensive study, involving six jet-finding algorithms, and the inclusion of the resulting rms deviations of results as additional uncertainties, represents a conservative procedure.

ACKNOWLEDGMENTS

We thank the personnel of the SLAC accelerator department and the technical staffs of our collaborating institutions for their outstanding efforts on our behalf. This work was supported by the U.S. Department of Energy and National Science Foundation, the UK Particle Physics and Astronomy Research Council, the Istituto Nazionale di Fisica Nucleare of Italy, the Japan-US Cooperative Research Project on High Energy Physics, and the Korea Research Foundation (Soongsil). We also thank A. Brandenburg, P. Uwer and L. Dixon for performing onerous QCD calculations for this analysis and for helpful contributions, as well as T. Rizzo for many useful discussions.

[1] H. Fritzsch, M. Gell-Mann, and H. Leutwyler, Phys. Lett. **47B**, 365 (1973); D. J. Gross and F. Wilczek, Phys. Rev. Lett. **30**, 1343 (1973); H. D. Politzer, *ibid.* **30**, 1346 (1973); S. Weinberg, *ibid.* **31**, 494 (1973).

[2] For a recent review of α_s measurements in e^+e^- annihilation see P. N. Burrows, in Proceedings of the XVII International Conference on Physics in Collision, Bristol, England, 1997, SLAC-PUB-7631.

[3] See e.g., M. Bilenky, G. Rodrigo, and A. Santamaria, Nucl. Phys. **B439**, 505 (1995).

[4] W. A. Bardeen, A. J. Buras, D. W. Duke, and T. Muta, Phys. Rev. D **18**, 3998 (1978); D. W. Duke, Rev. Mod. Phys. **52**, 199 (1980).

[5] DELPHI Collaboration, P. Abreu *et al.*, Phys. Lett. B **418**, 430 (1998).

[6] T. G. Rizzo, Phys. Rev. D **50**, 4478 (1994).

[7] TASSO Collaboration, W. Braunschweig *et al.*, Z. Phys. C **42**, 17 (1989); **44**, 365 (1989).

[8] L3 Collaboration, B. Adeva *et al.*, Phys. Lett. B **271**, 461 (1991); DELPHI Collaboration, P. Abreu *et al.*, *ibid.* **307**, 221 (1993); OPAL Collaboration, M. Z. Akrawy *et al.*, Z. Phys. C **65**, 31 (1995).

[9] ALEPH Collaboration, D. Buskulic *et al.*, Phys. Lett. B **355**, 381 (1995).

[10] OPAL Collaboration, R. Akers *et al.*, Z. Phys. C **60**, 397 (1993).

[11] SLD Collaboration, K. Abe *et al.*, Phys. Rev. D **53**, 2271 (1996).

[12] W. Bernreuther, A. Brandenburg, and P. Uwer, Phys. Rev. Lett. **79**, 189 (1997); A. Brandenburg and P. Uwer, Nucl. Phys. **B515**, 279 (1998).

[13] G. Rodrigo, A. Santamaria, and M. Bilenky, Phys. Rev. Lett. **79**, 193 (1997).

[14] SLD Design Report, SLAC-Report-273, 1984.

[15] SLD Collaboration, K. Abe *et al.*, Phys. Rev. D **51**, 962 (1995).

[16] M. D. Hildreth *et al.*, Nucl. Instrum. Methods Phys. Res. A **367**, 111 (1995).

[17] C. J. S. Damerell *et al.*, Nucl. Instrum. Methods Phys. Res. A **288**, 236 (1990).

[18] S. Brandt *et al.*, Phys. Lett. **12**, 57 (1964); E. Farhi, Phys. Rev. Lett. **39**, 1587 (1977).

[19] D. Axen *et al.*, Nucl. Instrum. Methods Phys. Res. A **328**, 472 (1993).

[20] T. Sjöstrand, Comput. Phys. Commun. **82**, 74 (1994).

[21] P. N. Burrows, Z. Phys. C **41**, 375 (1988); OPAL Collaboration, M. Z. Akrawy *et al.*, *ibid.* **47**, 505 (1990).

[22] SLD Collaboration, K. Abe *et al.*, Phys. Rev. Lett. **79**, 590 (1997).

[23] R. Brun *et al.*, Report No. CERN-DD/EE/84-1, 1989.
[24] JADE Collaboration, W. Bartel *et al.*, Z. Phys. C **33**, 23 (1986).
[25] D. J. Jackson, Nucl. Instrum. Methods Phys. Res. A **388**, 247 (1997).
[26] S. Bethke *et al.*, Nucl. Phys. **B370**, 310 (1992); Nucl. Phys. (to be published).
[27] Z. Kunszt *et al.*, Report No. CERN 89-08 **I**, 373 (1989).
[28] G. Marchesini *et al.*, Comput. Phys. Commun. **67**, 465 (1992).
[29] I. G. Knowles and G. D. Lafferty, J. Phys. G **23**, 731 (1997).
[30] N. Oishi, Ph.D. thesis, Nagoya University, 1998.
[31] A. Brandenburg (private communication).
[32] L. Dixon and A. Signer, Phys. Rev. Lett. **78**, 811 (1997); Phys. Rev. D **56**, 4031 (1997).
[33] L. Dixon (private communications).
[34] SLD Collaboration, K. Abe *et al.*, Phys. Rev. Lett. **80**, 660 (1998).